ELEVENTH EUROPEAN ROTORCRAFT FORUM

Paper No. 8

SHOCK FITTING APPLIED TO THE PREDICTION OF HIGH-SPEED ROTOR NOISE

Major John W. Rutherford

U.S. Army Aviation Research and Technology Activity-AVSCOM
Aeroflightdynamics Directorate
Ames Research Center
Moffett Field, CA

September 10-13, 1985

London, England

THE CITY UNIVERSITY, LONDON, EC1V OHB, ENGLAND

SHOCK FITTING APPLIED TO THE PREDICTION OF HIGH-SPEED ROTOR NOISE

Major John W. Rutherford
U.S. Army Aviation Research and Technology Activity
Aeroflightdynamics Directorate
Ames Research Center
Moffett Field, California 94035, U.S.A.

ABSTRACT

A shock fitting method applied to the transonic small disturbance (TSD) potential equation is described. This method is then applied to a simple, two-dimensional (2-D) rotating disturbance which is analogous to a shock radiating from the tip of a rotor blade in high-speed hover. A comparison is made between the results of this method and the more standard shock-capturing method. This comparison makes it clear that the effect of the results on the acoustic signature of the 2-D model is significant, and similar results can be expected when the method is extended to the three-dimensional (3-D) case.

1. NOMENCLATURE

a	speed of sound, m/sec
c	bump chord length, m
R	radius of model cylinder, m
r	cylindrical radial distance, m
t	time, sec
γ	ratio of specific heats
θ	angle measured in cylindrical coordinates
ϕ	velocity potential, m^2/sec
Ω	angular velocity, sec^{-1}

Subscripts

c	property of the chord
s	property of the shock
∞	free-stream condition

2. INTRODUCTION

The ability to predict the far-field acoustic signature of a high-speed rotor blade has met with limited success in the transonic regime. To date, researchers have used the Ffowcs-Williams and Hawkings Equation to predict rotor noise in the far field. This method requires detailed data for velocity and pressure in the region surrounding the blade tip. This information was obtained from finite-difference potential solutions of the flow field around a blade rotating at transonic tip speeds. This effort produced results which correlated well compared

with experimental rotor data taken in high-speed hover. These results were valid up to some limiting tip Mach number beyond which the results do not correlate well (refs. 1-3).

When viewed from a blade-fixed coordinate system (fig. 1), the velocity of the free stream increases linearly with radius. At some radius (defining the "sonic circle"), the free stream becomes sonic. The region outboard of the sonic circle is supersonic relative to the blade, while the region inboard is subsonic. At high tip Mach numbers, a region of supersonic flow, terminated by a shock, will form adjacent to and extend away from the blade surface in three dimensions. As the tip Mach number increases, the region of supersonic flow will grow larger until it finally connects with the outer supersonic region. When this occurs, a hyperbolic region will extend from the blade surface to the far field. Because of the highly radiative nature of this region, the shock will also escape to the far field, dramatically increasing the acoustic signature of the rotor. This phenomenon is known as "delocalization" (ref. 4), and it occurs at subsonic tip Mach numbers. The Mach number at which delocalization occurs appears to be the limiting Mach number at which theoretical prediction of the far-field acoustic signature no longer correlates well with experimental data. It is believed that the onset of the characteristic, impulsive "popping" noise of a rotor in high-speed flight is caused by this delocalization.

Delocalization has been investigated using a more basic 2-D model (ref. 5). A disturbance in the form of a circular-arc bump spanning the surface of a rotating cylinder is used as a computational model. The 2-D rotational-disturbance model maintains the same mechanism for propagation of the shock to the far field as that of the 3-D case. The relationship of the model to the 3-D rotor case can be seen in figure 2. The 2-D computational model is less complex to program and requires much less computer time to run.

As previously stated, velocity and pressure data in the region surrounding the blade must be obtained to determine the far-field signature. This means that the accuracy of the far-field solution depends directly on the accuracy of near-field data. The highly nonlinear nature of the flow field at the tip region of the blade requires the use of finite-difference methods to obtain the required data. This flow field contains weak shocks and the accurate representation of these shocks presents a significant problem. Finite-difference formulations tend to smear the shock over several grid points. This effect is more pronounced with increasing distance from the disturbance. If the shock is oblique to the grid, it can become smeared over many points. These problems make obtaining an accurate representation of the strongest source of far-field noise extremely difficult, and hence the prospects of accurate noise prediction are dismal.

3. MATHEMATICAL MODEL

The 2-D computational model is formulated using potential theory. This model minimizes computational requirements, while maintaining the essential propagation properties. Strictly speaking, the potential model does not conserve momentum in transonic problems. However, the shocks involved in this problem are typically so weak that the errors so caused are negligible--especially in the far field. Furthermore, the computational efficiency of a potential model is far greater than that of an Euler equation model. The small-disturbance approximation may be used to further simplify the model, even though it may be limited at some radial distance from the surface because it assumed small shock angles.

The governing equation used as the computational model is obtained by casting the potential equation in a reference frame that rotates with the circular-arc bump (fig. 3). When the classical small-disturbance approximation is invoked, only the lowest-order, nonlinear term is retained and the final equation may be written as follows (ref. 5)

$$\left[\left(\frac{\mathcal{R}}{y}\right)^2 - M_R^2 - (\gamma + 1)M_R^2 \frac{\mathcal{R}^2}{y^2}\right]\phi_x \phi_{xx} + \phi_{yy} + \frac{1}{y}\phi_y = 0 \qquad (1a)$$

where

$$M_R = \frac{\Omega R}{a_\infty}, \quad y = \frac{r}{c}, \quad \mathcal{R} = \frac{R}{c}, \quad x = \frac{\theta}{\theta_c} = \theta\mathcal{R}$$

The nonlinear sonic circle will be defined at the value of y where the coefficient of ϕ_{xx} changes sign.

An interesting feature of this rotational transonic small-disturbance equation is the $1/y^2$ dependence of the nonlinear term. As the equation is used at points further away from the surface, this term approaches zero and the equation becomes linear. The next higher-order term which could be retained results in a modified version, equation (1b). This modified equation remains nonlinear in the far field. However, tests of this equation show no significant difference from the results of equation (1a).

$$\left[\frac{\mathcal{R}^2}{y^2} - M_R^2 - (\gamma + 1)M_R^2 \frac{\mathcal{R}^2}{y^2}\phi_x\right]\phi_{xx} + \phi_{yy} + \frac{1}{y}\phi_y - 2M_R^2\phi_y\phi_{xy} = 0 \qquad (1b)$$

4. SHOCK FITTING VS. SHOCK CAPTURING

The usual method of solving equation (1a) is a method known as shock "capturing." This method is very desirable because there is no

explicit allowance made for the existence of a shock in the flow field. Rather, local-differencing schemes are employed to ensure stability in both elliptic and hyperbolic regions. During this process, shocks appear as high gradients, but not necessarily discontinuous parts of the solution. The result is that the shock is smeared over several grid points. The smearing occurs because the finite-difference schemes are based on Taylor-series expansions and can be valid only for continuous flow regions. Differencing across a shock will result in a locally incorrect approximation of the differential equation. For supersonic/subsonic shocks, the smearing will occur over three grid points, while for supersonic/supersonic shocks, the smearing may occur over as many as ten grid points. The shocks on a typical transonic fixed-wing surface are sufficiently strong so that the resolution over three grid points exceeds what can be experimentally measured. Therefore, smearing in this solution is not objectionable. However, for the problem of high-speed rotor noise, the radiative region of interest includes weak supersonic/supersonic shocks. This problem is further aggravated by the widening of the cylindrical grid as radius increases. The only way to improve the resolution of the shock is to add more points to the grid. This considerably increases the computation time and the computer storage requirements.

The transonic, small-disturbance equation can be cast in either conservative or nonconservative form. Equation (1) is the nonconservative form. This form is easier to implement, but mass is not conserved across the shock. The reason for this is the overlapping of differencing schemes when the shock forms the boundary between a supersonic region and a subsonic region. Stability of the numerical method requires that a backward- or upwind-differencing scheme be used in a hyperbolic flow region, while a central-differencing scheme is used in an elliptic region. To conserve mass across the shock, care must be taken to write and solve equation (1a) in the conservative form as follows

$$\frac{R}{y}\,\partial_x\left[\frac{R}{y} - M_R^2\,\frac{y}{R}\,\phi_x - \frac{\gamma+1}{2}\,\frac{R}{y}\,M_R^2\phi_x^2\right] + \frac{1}{y}\,\partial_y(y\phi_y) = 0 \qquad (2)$$

An alternative to the shock capturing method is to explicitly impose the shock-jump relation allowed by the transonic small-disturbance equation in the solution process. This procedure is known as shock "fitting." Such a method, formulated for the potential equation by Hafez and Cheng (ref. 6) is used in this study. This method relies on the a priori knowledge of the presence of a shock in the flow field, as well as its approximate location. The implementation of this method is outlined in the following steps:

1. The presence of a shock, as well as its approximate location, is determined from a captured solution, either conservative or nonconservative. The location of the shock is determined based on the location of the maximum positive gradient of the pressure coefficient on

each grid line of constant y. With the location known, the slope of the shock is also determined. From this initial solution, it is also possible to determine whether or not the shock has delocalized.

2. Solve the governing equation using the same capturing method up to the shock location. At the first grid point after the shock, solve for the velocity potential explicitly using the shock-jump relation. This relation, as will be seen, depends on the shock slope, the upstream velocity component in the streamwise direction, and the fact that the velocity potential is continuous across the shock. The value at this grid point will act as an internal boundary condition for solution of the equation downstream of the shock, which is computed using the capture method.

3. Once the flow-field solution is obtained, adjust the shock location using an unsteady geometric version of the shock-jump relation. This will ensure, before the next iteration, that the shock location agrees with the latest flow-field solution. Eventually, the shock will no longer have to be adjusted and a converged solution will be reached.

4. Impose continuity of the velocity potential across the shock. The movement of the shock during step 3 may result in a downstream grid point becoming an upstream grid point or vice versa. If this is the case, the value must be corrected by extrapolation to ensure a continuous potential distribution.

5. Solve the governing equation by iteration until a steady-state shock location is determined.

Shock fitting conserves mass across the shock because the jump relation is imposed at the point just downstream of the shock. As will be seen, this relation is derived from the conservation form of the equation. An important rule in implementing the shock-fitting method is not to difference across the shock from either side.

4.1 Shock-Jump Relation

The shock-jump relation allowed by the transonic small-disturbance equation is the key element in the application of the shock-fitting algorithm. Equation (2), which is written in conservative form, is of the form

$$\vec{\nabla} \cdot \vec{B} = 0$$

where

$$\vec{B} = \vec{B}_x + \vec{B}_y$$

and

$$\vec{B}_x = \left\{\left(\frac{\mathcal{R}}{y} - M_R^2 \frac{y}{\mathcal{R}}\right)\phi_x - \frac{\gamma + 1}{2} \frac{\mathcal{R}}{y} M_R^2 \phi_x^2\right\}\hat{i}$$

$$\vec{B}_y = (\phi_y)\hat{j} \tag{3}$$

Making use of the shock-tangency condition, and applying the divergence theorem, the resultant jump condition is

$$-\left(\frac{\mathcal{R}^2}{y^2} - M_R^2\right) + (\gamma + 1)M_R^2 \frac{\mathcal{R}^2}{y^2} \langle \phi_x \rangle = \left(\frac{dx}{dy}\right)_s^2 \tag{4}$$

where $\langle\ \rangle$ represents the average across the shock.

When implementing the shock-jump relation, it is necessary to give special treatment to certain points in the vicinity of the shock location (ref. 6). Moving in the streamwise direction, the last point prior to the shock location could look like that shown in figure 4. As can be seen, the computational molecule for this point contains the point A, which lies downstream of the shock. So as not to violate the "rule of forbidden signals," it is necessary to use a value for the potential at point A which is extrapolated from the upstream side of the shock. Then, the point ahead of the shock may be computed in the usual upwind manner. If the shock is supersonic/supersonic, then the point after the shock point, B, must be differenced downstream as shown in figure 5. Once again, care must be taken not to difference across the shock. Since the shock location is known, and ϕ must be continuous across the shock, the value of ϕ at the shock is extrapolated from upstream data. Just downstream of the shock, ϕ_x has already been computed and serves as a Neuman boundary condition. No special treatment need be paid to this point if the shock is supersonic/subsonic.

4.2 Shock Movement

The requirement to update the shock location requires a form of the jump relation in which the shock motion is a function of the upstream and downstream flow conditions (ref. 7). Such a relation can be obtained from the unsteady small-disturbance equation.

$$\partial_x A \phi_t = \frac{\mathcal{R}}{y} \partial_x \left[\left(\frac{\mathcal{R}}{y} - M_R^2 \frac{y}{\mathcal{R}}\right)\phi_x - \frac{\gamma + 1}{2} \frac{\mathcal{R}}{y} M_R^2 \phi_x^2\right] + \frac{1}{y} \partial_y y \phi_y \tag{5}$$

The divergence theorem is applied and using the relation

$$[\![\phi_t]\!] = -\frac{dx}{dt} [\![\phi_x]\!] \tag{6}$$

the time dependency of ϕ can be replaced by a spacial differencing, where $[\![\ ]\!]$ represents the difference across the shock. This time factoring out ϕ_x ultimately results in the following geometric relation

$$2M_R^2 \frac{\partial x}{\partial t} + \left(\frac{dx}{dy_s}\right)^n \frac{\partial x}{\partial y_s} = -\left(\frac{R^2}{y^2} - M_R^2\right) + (\gamma + 1)M_R^2 \frac{R^2}{y^2} \langle \phi_x \rangle \tag{7}$$

This is of the form

$$A \left(\frac{\partial x}{\partial t}\right)_s + B \left(\frac{\partial x}{\partial y}\right)_s = C \tag{8}$$

It can be solved using a variety of methods, but in this instance, an implicit trapezoidal scheme is used to avoid any restriction on the size of the time step.

$$x_k^{n+1} = \left[x_k^n + \frac{C\ \Delta t}{A} + \frac{B\ \Delta t}{A\ \Delta y} x_{k-1}^{n+1}\right] \cdot \left(1 + \frac{B\ \Delta t}{A\ \Delta y}\right)^{-1} \tag{9}$$

Even so, there is an upper limit set not by the stability of the equation, but by the amount of shock movement allowed by each iteration. A large movement of the shock causes instability in the next iteration of the solution. Since the time step is not real, Δt can be set to any value desired by the user. Here, $\Delta t = 0.5$ is used. Once the new shock location is found, it is necessary to use a data smoothing technique, such as a least-squares fitting, to ensure a continuous shock slope. A key feature of equation (8) is that the shock moves based on the right-hand side of the equation, which is dependent on the solution to the flow field upstream and downstream of the shock. From equation (4), the right-hand side of equation (8) defines the inverse of the shock slope squared. As the iterations are continued, the slope defined by the right-hand side of equation (8) should become equal to the slope on the left-hand side. When this has occurred, the solution is said to be converged.

The movement of the shock is the most difficult portion of the shock-fitting method to implement. The slope of the shock must be kept continuous in some manner. The oblique portion of the shock beyond the sonic circle exhibits extreme sensitivity to shock angle. In one case, the difference in shock angle of 0.4 of a degree was enough to totally destroy the solution. This was a result of the shock-jump relation yielding a shock slope approaching the slope of the linear characteristic as y increases. When this happens, the coefficient of $\langle \phi_x \rangle$ in equation (4) becomes very small and any small deviation in the shock slope from the characteristic value results in large values for $\langle \phi_x \rangle$.

5. RESULTS

To ensure that the shock-fitting method was implemented correctly, a step-by-step progression of test cases was accomplished. The first case consisted of a wedge in supersonic rectilinear flow with a free-stream Mach number of 1.15. This case confirmed the logic necessary to fit a supersonic/supersonic shock. The result, shown in figure 6, was an attached shock at the leading edge. A glance at the pressure distribution shows a remarkable clarity of the shock as compared to the captured case. In the second case, the result is a detached bow shock for a circular-arc bump translating at a Mach number of 1.15. Figure 7 shows the shock location displacement from the captured solution, while figure 8, again, demonstrates the resolution of the shock. Note that the solution also shows a shock at the trailing edge. The fitting method was not used on this shock. This case is important because it demonstrated the shock structure present for the rotating, delocalized case which has a supersonic/subsonic portion and a supersonic/supersonic portion.

Once confidence in the implementation of the shock fitting method was gained from the preceding test cases, the method was applied to the model rotational problem. The rotating circular-arc bump is depicted by the following conditions: 1) thickness is 6%, 2) radius/chord ratio is 10, and 3) rotational Mach number is 0.9. Both Alternating Direction Implicit (ADI) and Successive Line Over Relaxation (SLOR) schemes were tried and worked successfully, with ADI having the expected convergence rate advantage. Figure 9 shows the comparison of the captured shock location with that of the fitted solution. Since the captured solution is formulated using the nonconservative form, the shock is slightly forward of the fitted solution which conserves mass across the shock. This is to be expected within the sonic circle. Beyond the sonic circle, there is no conservation question since there is no need to use a switched-differencing scheme. The shock moves forward in the course of correcting the extreme smearing which is exhibited by the captured solution. Figures 10-12 show the comparison of captured and fitted pressure data at different radii from the surface of the cylinder. In figure 10, the results show very little difference in amplitude or in the discontinuous nature of the shock. As the distance from the disturbance increases (figs. 11 and 12), the solutions become much different. The captured solution shows marked smearing, while the fitted solution not only shows a sharp discontinuity, but also marked increase in the amplitude of the pressure.

Figure 13 gives an overview of the flow field and compares the captured and fitted solutions by using isomach lines. Here, it is clear that the shock maintains a sharp discontinuity throughout the flow field.

6. CONCLUSIONS

The 2-D computational model using the TSD equation models the delocalization phenomenon well. It is simple in all computational aspects, yet still provides the mechanism which allows shocks to propagate to the far field from a subsonically rotating disturbance. Applying the shock-fitting algorithm to the solution process changes the nature of the resulting flow field significantly. The discontinuous nature of the shock is maintained throughout the field and well beyond the sonic circle. In the process of sharpening this discontinuity, the amplitude of the shock increases. Both of these factors are important in predicting the acoustic signature in the far field, since the shock is the primary near-field noise source.

The implementation of the shock-fitting scheme for the 3-D rotor case is being pursued. Recently measured, experimental rotor data will be used to verify the computed near-field acoustic signature. This will validate the accuracy of the computed, near-field data necessary to predict the far-field signature.

The shock-fitting method has some minor drawbacks. The complexity of programming is increased because of the logic necessary to accommodate the shock points. A stretched grid may still limit the resolution of a shock far away from the disturbance; however, the solution will always show a considerably sharper shock than the captured method. The TSD equation may also be of limited use in the far field, but it may be adequate for determining the desired flow properties in the near field.

When applied to the 3-D case, the solution should provide insight into the theoretical prediction of the far-field acoustic signature for a rotor operating at tip Mach numbers beyond the delocalization Mach number.

ACKNOWLEDGMENTS

The author wishes to express his sincere appreciation to several people who gave their time and provided guidance and invaluable advice during the pursuit of this research: Frank Caradonna, Fred Schmitz, Yung Yu of the U.S. Army Aviation Research and Technology Activity, Aeroflightdynamics Directorate, and Mohammed Hafez of the NASA Langley Research Center. A special thanks is given to Miss Cathy Druffel of the U.S. Army Aeroflightdynamics Directorate for the outstanding computer graphics support provided for both this paper and its oral presentation.

REFERENCES

1. Schmitz, F. H.; and Yu, Y. H.: Transonic Rotor Noise--Theoretical and Experimental Comparisons. Vertica, vol. 5, 1981, pp. 55-79.

2. Shenoy, K. R.: A Semiempirical High-Speed Rotor Noise Prediction Technique. Presented at the 38th Annual National Forum of the American Helicopter Society, Anaheim, California, May 4-7, 1982.

3. Boxwell, D. A.; Yu, Y. H.; and Schmitz, F. H.: Hovering Impulsive Noise: Some Measured and Calculated Results. Vertica, vol. 3, 1979, pp. 33-45.

4. Yu, Y. H.; Caradonna, F. X.; and Schmitz, F. H.: The Influence of the Transonic Flow Field on High-Speed Helicopter Impulsive Noise. Paper 58, Presented at the 4th European Rotorcraft and Powered Lift Aircraft Forum, Stresa, Italy, 1978.

5. Rutherford, J. W.: The Aerodynamics and Aeroacoustics of Rotating Transonic Flow Fields. Presented at the 39th Annual National Forum of the American Helicopter Society, St. Louis, Missouri, May 1983.

6. Hafez, M. M.; and Cheng, H. K.: Shock-Fitting Applied to Relaxation Solutions of Transonic Small Disturbance Equations. AIAA Journal, vol. 15, no. 6, June 1977, pp. 786-793.

7. Hafez, M. M.; and Murman, E. M.: A Shock Fitting Algorithm for the Full Potential Equation. Presented at the AIAA 3rd Computational Fluid Dynamics Conference, Albuquerque, New Mexico, June 1977.

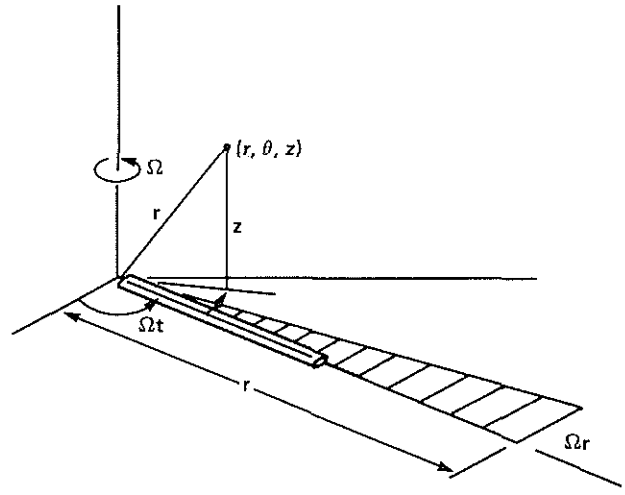

Fig. 1. Blade-fixed coordinate system from reference 4.

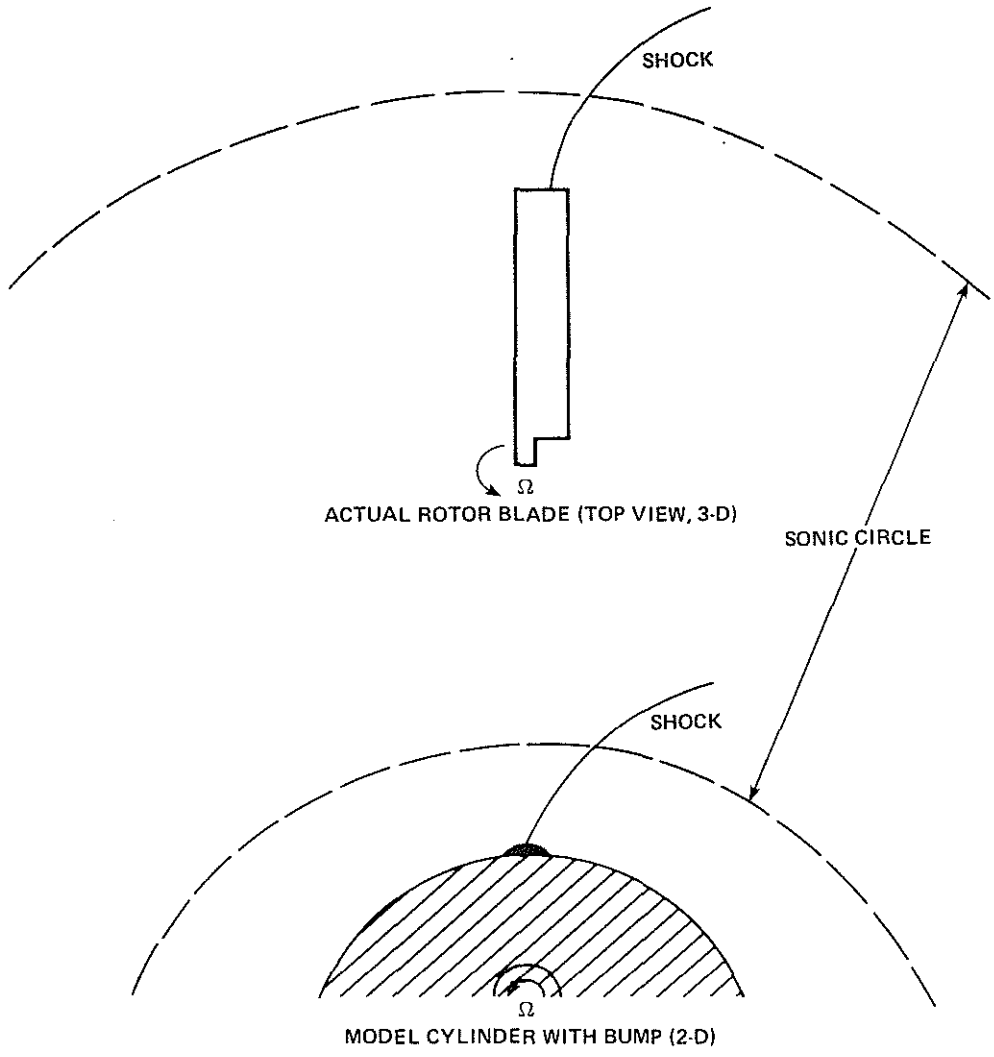

Fig. 2. Comparison of computational model to actual rotor.

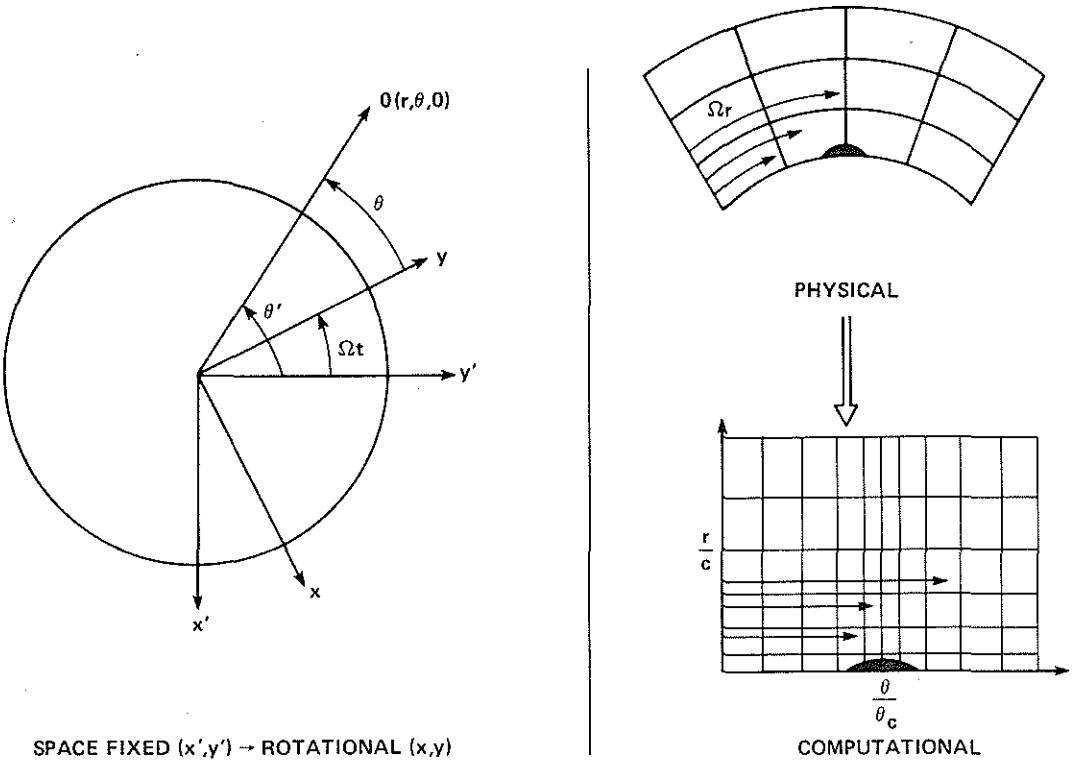

Fig. 3. Coordinate transformation of computational model.

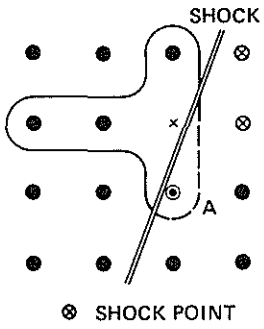

Fig. 4. Differencing upstream of a shock.

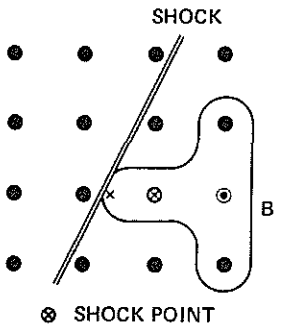

Fig. 5. Differencing downstream of a supersonic/supersonic shock.

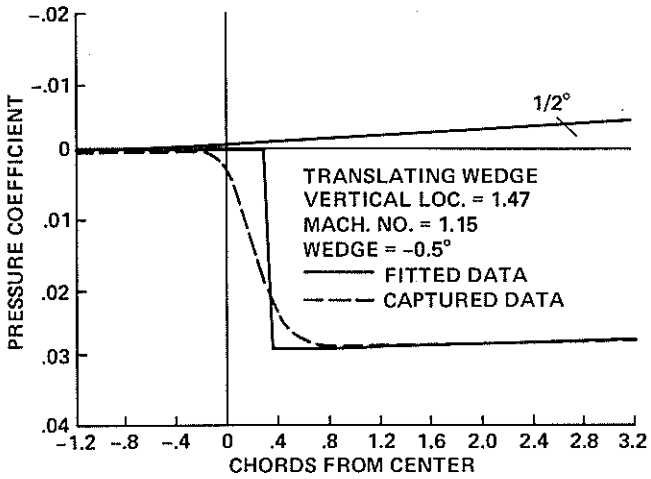

Fig. 6. Comparison of fitted and captured solutions for a wedge at Mach number = 1.15.

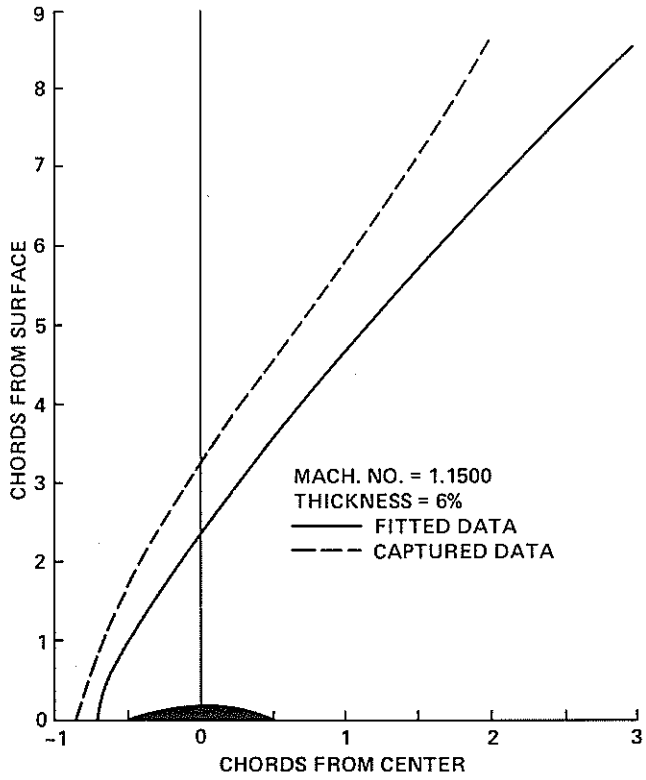

Fig. 7. Comparison of shock locations for a 6% circular arc translating at Mach number = 1.15.

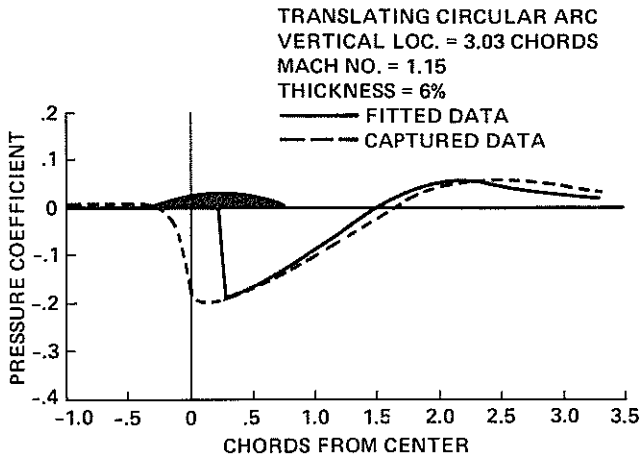

Fig. 8. Comparison of fitted and captured solutions for a 6% circular arc translating at Mach number = 1.15. Solution is 3.03 chords above the surface. (Rear shock is not fitted.)

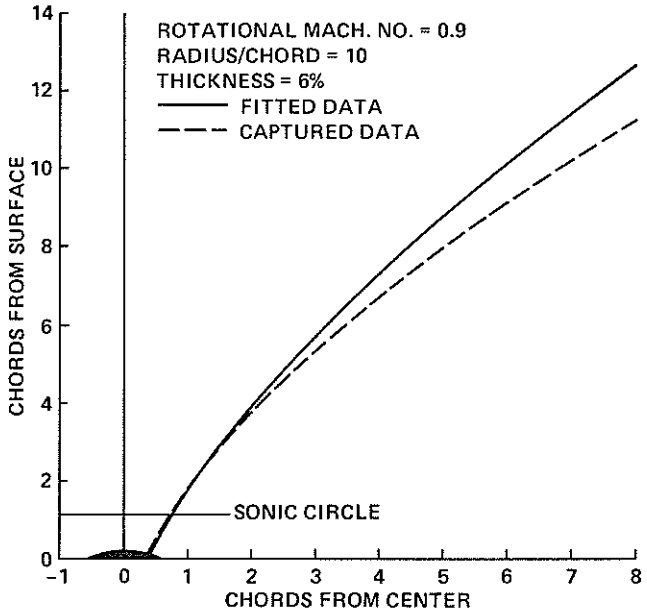

Fig. 9. Comparison of shock locations for a 6% circular arc rotating at Mach number = 0.9.

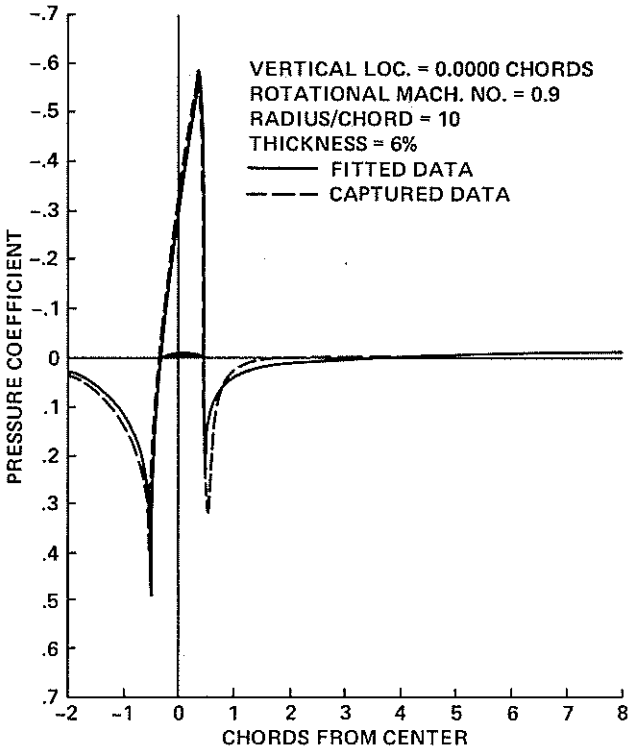

Fig. 10. Comparison of fitted and captured solutions for a 6% circular arc rotating at Mach number = 0.9; y = 0.

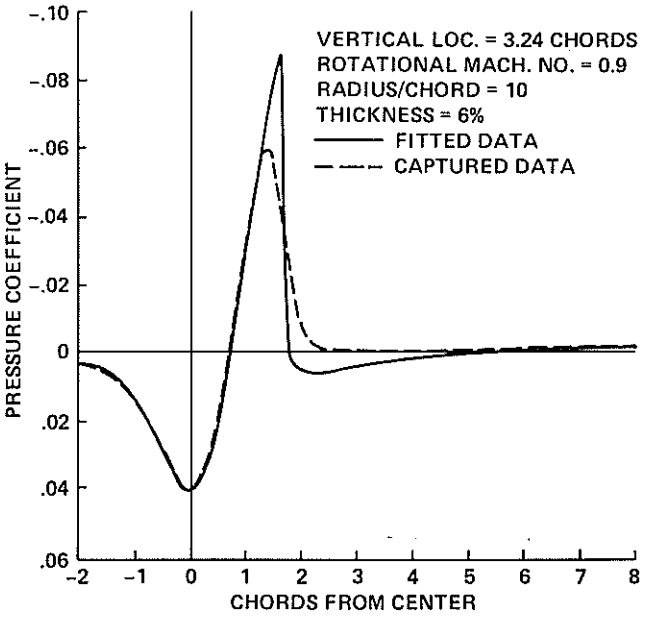

Fig. 11. Comparison of fitted and captured solutions for a 6% circular arc rotating at Mach number = 0.9; y = 3.24 chords.

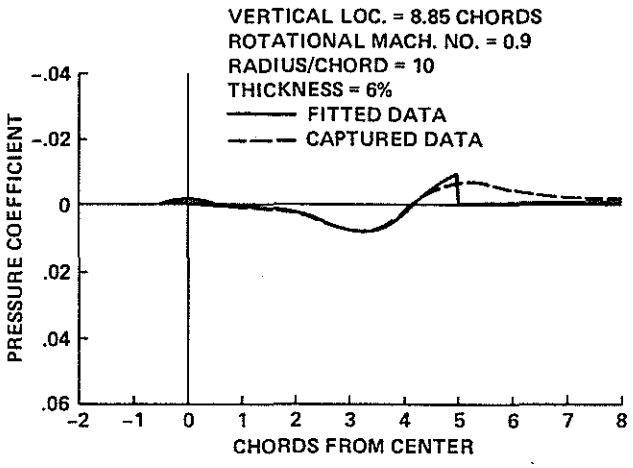

Fig. 12. Comparison of fitted and captured solutions for a 6% circular arc rotating at Mach number = 0.9; y = 8.85 chords.

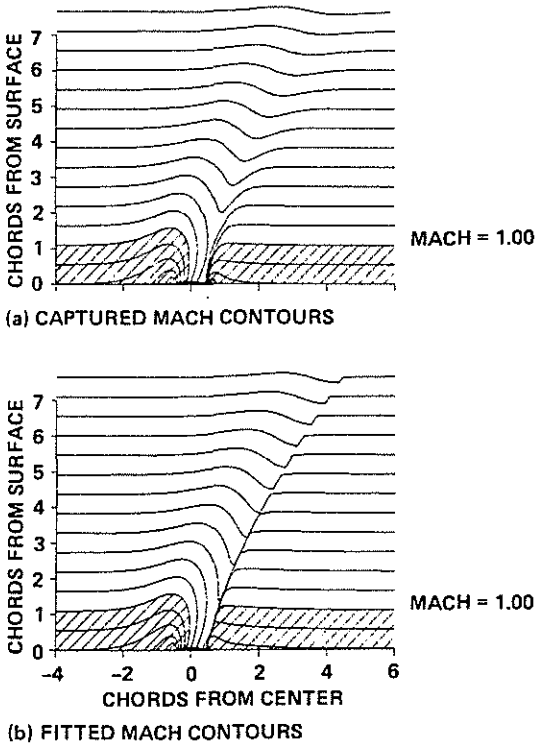

Fig. 13. Isomach contours comparing a captured solution and a fitted solution for a 6% circular arc rotating at Mach number = 0.9.